ARTICLE

In vitro exploration of the synergistic effect of alternating magnetic field mediated thermo-chemotherapy with doxorubicin loaded dual pH- and thermo-responsive magnetic nanocomposite carriers

Received 15th August 2020,
Accepted 17th September 2020
DOI: 10.1039/D0TB01983F

Lilin Wang,[a,b] Aziliz Hervault,[a,b] Paul Southern, [b,c] Olivier Sandre, [e] Franck Couillaud [d] and Nguyen Thi Kim Thanh* [a,b]

ABSTRACT: Nanoparticle induced hyperthermia has been considered as a promising approach for cancer treatment for decades. The local heating ability and drug delivery potential highlight a diversified possibility in clinical application, therefore a variety of nanoparticles that has been developed accordingly. However, currently, only a few of them have been translated into clinical stage indicating the 'nanoparticle medically underserved' situation, which encourages their comprehensive biomedical exploration. This study presents a thorough biological evaluation of previous well-developed dual pH- and thermo- responsive magnetic doxorubicin-nanocarrier (MNC-DOX) in multiple cancer cell lines. The cytoxicity of the nanocomposites has been determined by the MTT assay on primary cell lines. The histology and fluorescence microscopy imaging revealed the efficiency of various cellular uptake of nanocarriers in different cell lines. The IC_{50} of MNC-DOX is significantly higher than free DOX without alternative magnetic field (AMF), which implied the potential to lower the systemic cytotoxicity in clinical research. The concurrent thermo-chemotherapy generated by this platform has been successfully achieved under AMF. Promising effective synergistic results have been demonstrated through in vitro study in multi-model cancer cell lines via both trypan blue exclusion and bioluminescence imaging methods. Furthermore, the two most used magnetic hyperthermia modality, namely intracellular and extracellular treatments have been compared on the same nanocarriers in all 3 cell lines, which showed treatment after internalization is not required but preferable. These results lead to the conclusion that this dual responsive nanocarrier has extraordinary potential to serve as a novel broad-spectrum anticancer drug and worth to be pursued for potential clinical applications.

Introduction

Hyperthermia has been considered as a promising therapy for cancer since the last century. Ideally, the tumour compartments with uncontrolled growth cancer cells can be killed solely without influence on the function of surrounding healthy cells. Especially, localized hyperthermia has been demonstrated that it can eradicate the carcinoma cells via multiple ways. On the cellular level, the thermal cytotoxicity itself directly kills the cancer cells via irreversible cytoplasmic and membrane proteins denaturation on the molecular level,[1,2] the absorbed heat provokes numerous apoptosis related cellular pathways, which include cytochrome C released mitochondria apoptosis and TNF-related apoptosis-inducing ligand death receptors DR4, DR5[3,4], or non-apoptotic cell death such as caspase inflammation enzyme activation.[5] Furthermore, the heat shock proteins can also serve as a target motif on the cell membrane for activating and augmenting the immune cell against the targeted cells.[6] However, as the clinical results suggest hyperthermia should be considered as an adjuvant therapy rather than first-line treatment alone at the moment.[7–10] The increased interests in promoting localized hyperthermia into conventional cancer treatment had been hampered for a long time until the encouraging synergistic results of the combinational thermo-chemotherapy and thermo-radiotherapy have been revealed.[9,11–13]

Generally, the main reason for both chemotherapy and radiotherapy failure is attributed to an intricate tumour microenvironment. An advanced stage of solid tumour is characterized as inefficient blood flow, acidic pH and elevated

[a.] Biophysics Group, Department of Physics &Astronomy, University College London, Gower Street, London, WC1E 6BT, UK.
[b.] UCL Healthcare Biomagnetic and Nanomaterials Laboratories, 21 Albemarle Street, London, W1S 4BS, UK. Email: ntk.thanh@ucl.ac.uk
[c.] Department of Medical Physics and Biomedical Engineering, University College London, Gower Street, London, WC1E 6BT, UK.
[d.] Molecular Imaging and Innovative Therapies (IMOTION), Univ. Bordeaux, EA7435, Bordeaux, 33000, France.
[e.] Laboratoire de Chimie des Polymères Organiques (LCPO), Univ. Bordeaux, CNRS, Bordeaux INP, UMR 5629, 33600 Pessac, France.
Electronic Supplementary Information (ESI) available: [details of any supplementary information available should be included here]. See DOI: 10.1039/D0TB01983F

Author manuscript version

interstitial fluid pressure due to the cancer angiogenesis caused defective vasculature system. Unlike uniform chromosomal damage caused by the ionizing radiation that can be significantly enhanced by the thermal increased partial O_2 pressure and increased blood flow,[14] the factors and mechanisms involved in the thermo-sensitization of chemotherapy are far more complicated, which impeded its utilization. The different classes of drugs interaction with thermal effect undergo diverse mechanism to suppress cell proliferation.[1] Apart from that, different tumour types, diverse thermo-doses, and approaches of heat implementation also contributed to the thermo-chemo sensitisation. One of the assumptive mechanisms is the localized intra/intercellular drug concentration increased by the thermotherapy. The heat exposure in tumour area not only can elevate drug penetration along with increased cell membrane permeability and enlarging the size of fenestrations, but also increase blood perfusion flowrate to reduce physiological barrier, which is caused by the interstitial fluid pressure.[11,15] However, this benefit could be eliminated when the regional or whole body temperature rises, thus for thermo-chemotherapy, the thermal boosting is critically constrained by the temporal and spatial implementation. Therefore, compared with the conventional hyperthermia approach like with radiofrequency electrodes implanted in the tumour, utilization of magnetic nanoparticles (MNPs) for magnetic hyperthermia, provides a promising and less invasive solution for concurrent chemotherapy. The high surface to volume ratio of magnetic nanoparticle facilitates the feasibility of drug loading. Once adequate amount of nanoparticles is accumulated in the tumorigenic region via either enhanced permeability and retention (EPR) effect or external magnetic attraction, the AMF application with high tissue penetration could provide hyperthermia and chemotherapy simultaneously.[16–19]

Hundreds of syntheses of MNPs have been designed since 1957, when the first experimental reported study by Gilchrist et al. in animal (dogs) revealed the feasibility of using MNPs in radiofrequency magnetic hyperthermia.[20] However, in the past six decades, only few of them have undergone to clinical trials and the most successful case is with Magforce™ company whose treatment NanoTherm® has been approved in June 2010 to go into the high grade glioblastoma brain cancer European market (yet only when combined with conventional radiotherapy), which highlights that the MNPs have been highly underserved.[21,22]

A comprehensive biomedical investigation about MNPs is still needed to make magnetic hyperthermia therapy to be accessible to wider population. One of the unsolved issues is to determine which magnetic hyperthermia implementation method is superior:[23] intracellular hyperthermia which means that the nanoparticles either have been internalized into the cells or tightly deposited onto the cells, and then heated the cells directly; or extracellular hyperthermia, indicating that the thermal damages are produced through the extracellular matrix (ECM) temperature elevation or ECM mechanical disruption.[24] The proponents for intercellular hyperthermia demonstrated that it could provide a destructive effect despite the absence of macroscopic temperature increase,[25–29] like obtained by with intra-tumour injection and the extracellular approach. However, the effects varied among reported work in the literature. Besides, compared with extracellular strategies, the achievable thermal dose of intracellular hyperthermia is restricted by the insufficient internalization of nanoparticles.[30,31] This issue becomes more complicated when introducing other parameters, such as different chemotherapy drugs and nanoparticle compositions into the system. To date, there are not many investigations on how intracellular and extracellular magnetic hyperthermia could influence the chemosensitisation effect, particularly with the same type of nanoparticles.

This study presents, for the first time, i) a comprehensive biological evaluation of our previously well-developed dual pH- and thermo- responsive polymer-coated magnetic doxorubicin-nanocarrier (MNC-DOX), ii) multidirectional assessments on the thermal provoked synergistic effects of intracellular / extracellular hyperthermia with the same type of DOX loaded magnetic nanocarrier in multi-model cancer cell lines. The magnetic iron oxide cores were synthesized by microwave method and conjugated with DOX *via* pH-cleavable imine bonds by a thermo-responsive copolymer. Chemical and physical characterisation and *ex vivo* drug release pattern of this smart nanocarrier have been previously described by some of us.[32] In the present study, the biocompatibility of the nanocarrier is demonstrated in a primary immortalized murine fibroblast cell line, which is recommended by ISO10993-1:2009 procedure to assess biocompatibility of medical devices.[33] Then the cellular uptake of MNC in both human breast carcinoma (MCF-7) and glioblastoma (U-87) cell lines have been visualized by histology and fluorescence microscopy at different time points and quantitated *via* Superconducting Quantum Interference Device (SQUID) magnetometry. The half maximal inhibitory concentration (IC_{50}) values of MNC-DOX in all cell lines have been calculated and used to guide the loading during the following combination therapy. In order to acquire comprehensive results, three different cancer cell lines have been investigated: MCF-7 (human breast carcinoma), U-87 (human glioblastoma) and RM1-CMV-LucF (bioluminescent murine prostate cancer cells): for each cell line, approx. the same amount of internalized nanoparticle that has been calculated was loaded to the cells just before hyperthermia (thus without uptake) in the “direct treatment” group, which was used to compare with the “internalized” group. Furthermore, the temperature influence on magnetic thermo-chemotherapy has also been analysed by varying different amounts of nanoparticles in the direct / extracellular heating experiment.

published version at https://doi.org/10.1039/D0TB01983F

Author manuscript version

Author manuscript version

Results and discussion

Synthesis of the thermal and pH- sensitive nanocarriers

Briefly, TEM images indicated that, after their synthesis, the bare spherical iron oxide cores had an average size of 13.3 ±2.2 nm. The saturation magnetization of it at 300 K was 70 emu·g^{-1}. The successful conjugation of the MNCs, which contained 8.1% of the P(DEGMA-*co*-PEGMA-b[TMSPMA-*co*-VBA]) copolymer according to thermogravimetric analysis, have been confirmed by Fourier transformed infra-red spectroscopy. This copolymer was designed to have a thermosensitive block of diethylene glycol methacrylate and PEG methacrylate with a transition above physiological temperature. The second block possesses units with trimethoxy silane groups for grafting onto iron oxide surface by sol-gel reaction and vinylbenzaldehyde comonomer for conjugation to DOX amine group into a pH-sensitive imide bond.[30] With the help of this hydrophilic polymer coating, the hydrodynamic size of the nanocarrier as measured by dynamic light scattering (DLS) in aqueous media decreased from 194 nm to 120 nm.[30]

Cellular biocompatibility and uptake of MNCs.

In this work, the name "MNCs" refers to the P(DEGMA-*co*-PEGMA-*b*[TMSPMA-*co*-VBA]) polymer coated magnetic NPs. In order to apply these nanocarriers in medical applications, crucial factors such as biocompatibility and cellular uptake have been evaluated in multiple cancer cell lines. Nanoparticles with good biocompatibility is about whether they would induce any degree of toxicity, carcinogenicity or immunogenic response to the biological system.[34] Normally the physical and chemical properties of nanoparticles such as their size, shape, structure, hydrophilicity, hydrophobicity and charge, determine the cytotoxicity, but in a biological system the surface coating plays a vital role in the biocompatibility.[35,36] In our system, the magnetic core was composed of FDA approved material, magnetite, with designed physical properties to be bio-friendly; the thermal and pH sensitive hydrophilic coating contained widely used PEG side chains to prolong the systemic circulation time and prevent the aggregation.[37] Thus, the biocompatibility has been assured through this preliminary assay, as expected (Figure 1).

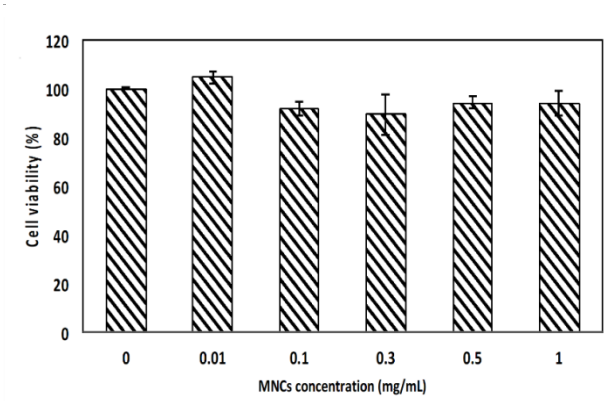


Figure 1. Biocompatibility study by MTT assay on L929 murine fibroblast cells with increasing concentration of MNCs.

Doxorubicin being a widely used chemotoxic drug in cancer treatment, we used it in order to evaluate whether our MNCs-DOX conjugated system had the potential to benefit patients with different types of cancer. The performances of this system had been accomplished for human glioblastoma U-87 cell line and human breast carcinoma MCF-7 cell line in parallel.

Therefore, the cellular uptake ability of the nanocarriers in both these cell lines had been visualized *via* histology staining. After incubation with the MNCs ranging from 0.1 mg/mL to 1.0 mg/mL after 4 h or 24 h, the MCF-7 breast cancer cell line and the U-87 glioblastoma cell line were counterstained with nuclear red dye, once the iron oxide nanoparticles were stained with Prussian blue (Figure 2). In both cell lines, the presence of Prussian blue staining suggested that the MNCs not only got internalized inside the cells, but also the uptake clearly depends on both the nanoparticle concentration and the exposure time. The U-87 cells appeared to obtain more MNCs as compared to the MCF-7 cells at high concentration and incubation time. This result is consistent with other studies that the nanoparticle uptake capability varies among different kind of cells and tissues,[38,39] e.g. 400 pg iron oxide per cell,[28] the uptake by U-87 cells being even higher, up to 800 pg iron oxide per cell for certain PEGgylated multicore MNCs.[40] However, these 2D images are produced by light microscopy, which not only cannot certainly distinguish the internalized MNCs or those that have been only deposited onto the cell membrane, but also cannot quantify these nanoparticles. Meanwhile, a high cellular capturing of nanoparticles, be they internalized or tightly deposited, is directly corresponding to a higher therapeutic efficiency. Thus, precise method to quantify the MNCs that have been captured by each cell lines is necessary for the following comparison of the therapeutic conducting approaches. Elemental analysis by ICP-MS is a good technique to quantify the internalized Fe content. However, it cannot distinguish between the endogenous iron cations that may already be there in the cell and the incubated nanoparticles. SQUID magnetometry is the only technique that characterizes

published version at https://doi.org/10.1039/D0TB01983F

Author manuscript version

Author manuscript version

exclusively the magnetic iron oxide nanoparticles in the biological system. Thus, the magnetic measurements of cells loaded with MNCs have been carried out by SQUID magnetometer measurements for quantification (Table 1). Comparison of the nanoparticle cellular internalization *via* both techniques has confirmed that cellular uptake of U-87 cells was higher than that of MCF-7 cells.

Table 1. MNC uptake quantification of Fe_3O_4 in pg/cell for human glioblastoma U-87 cells and human breast adenocarcinoma MCF-7 after incubation for 4 h and 24 h at different concentrations of MNCs solution.

Cell line	Time (h)	MNCs concentration (mg/mL)				
		0.01	0.05	0.10	0.50	1.00
MCF-7	4	/	/	1	3	6
	24	/	/	2	5	13
U-87	4	/	2	7	15	32
	24	2	6	12	55	125

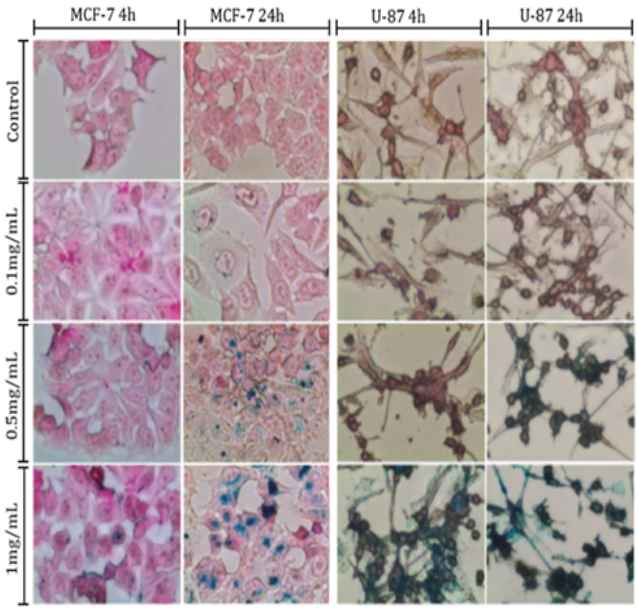


Figure 2. Microscope images of human glioblastoma U-87 cells and human breast adenocarcinoma MCF-7 loaded with MNCs after 4 h and 24 h of incubation with a solution containing different concentration of MNCs. Cells were counterstained with Prussian blue and nuclear fast red dyes.

Apart from the MNCs internalization, the intracellular localization of DOX is also critical in designing nanocarrier anticancer activity, as the therapeutic efficiency of this system is also determined by the DOX inhibition of the topoisomerase enzyme in the nucleus through binding to the tumour cell chromosome.[41,42] Hence, internalization of DOX, exhibiting an intrinsic red fluorescence, in U-87 and MCF-7 cells after incubation with either free DOX or MNCs-DOX, has been assessed by fluorescence microscopy (Figure 3).

Generally, the results revealed that the overall DOX accumulation of MNC-DOX for short term incubation *in vitro* was efficient for both cell lines but seems lower than for the free drug, while the patient's ultimate clinical outcome should benefit from the endocytic drug uptake and thermo-acidic dual controlled release pattern of the MNCs-DOX. The intracellular signals of free and encapsulation form of DOX in both cell lines were detectable even just after 3 h of incubation, and the signal intensities were amplified with increased incubation time. However, comparison between the free DOX and MNCs-DOX at each time points within same cell lines indicated that signal of free DOX was significantly stronger than with the nanoparticle loaded system, which implies that the free DOX has quicker and higher cellular accumulation in *in vitro* cultures. Besides, the DOX intensity from MCF-7 cells was lower than U87 implying that the U87 cell lines can engulf more DOX-MNCs, which is comparable to the observed cellular uptake of this nanocarrier as demonstrated by the previous dye staining and SQUID magnetic measurements.

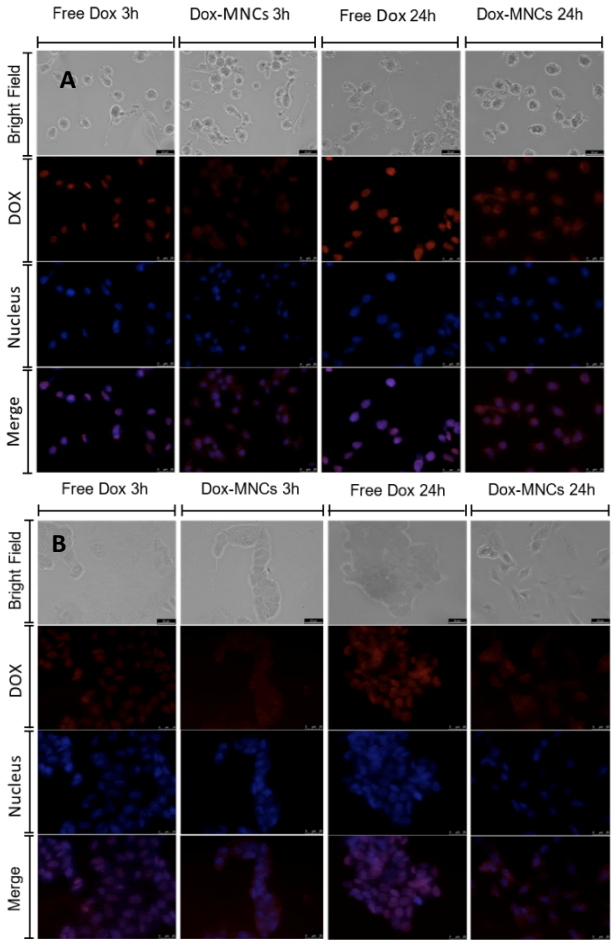


Figure 3. Fluorescence images of U87 cells (A) and MCF-7 cells (B) after 3 h and 24 h of incubation with either free DOX or DOX-MNCs. Cell nuclei were counterstained with blue dye DRAQ5. Scale bar: 20 µm.

published version at https://doi.org/10.1039/D0TB01983F

Author manuscript version

Author manuscript version

Furthermore, merging the DOX signal with blue emitting nucleus indicator DRAQ5 exposed the detailed intracellular localisation of DOX *in vitro*. It showed that the free DOX was rapidly accumulated in cell nucleus whereas our nanoparticle conjugated DOX was mainly captured in the cytoplasm even after 24 h incubation. These evidences are not only consistent with the other published nanostructure based DOX delivery pattern, by which the nano-structure based carriers are predominantly up-taken by the slower endocytosis pathway into endosomes rather than by the rapid passive diffusion that free DOX tends to go through; but also these experimental results verified that our system is an efficient drug delivery system as what demonstrated in our previous *ex vitro* cumulative drug release profiles.[43–46] Only small proportion of DOX was released from the endocytic organelle due to the gradually hydrolysis of Schiff base linkage bond between the drug and polymer, most of the drug still remaining in the cytoplasm within the stable MNCs carrier until the temperature stimulus has been applied.[32] Normally, the particles between 10 to 100 nm can internalized into the cells easily and fast with either clathrin-mediated endocytosis or *caveolae*-mediated endocytosis.[47,48] However, studies revealed that particles from hundreds of nanometers up to 5 μm in size can enter cells through macropinocytosis, characterized by ruffles that formed on the cell membrane that protrude to engulf the larger particles.[49] In our study, the nanocarriers have a hydrodynamic size of 120 nm with PDI of 0.16.[30] This means the suspensions have a broad range of size distribution, which contains particles both under the 100 nm threshold and above it. Thus, these nanocarriers may enter the cells under different pathways depending on their size.

Therefore, our drug delivery system on the one hand has the potential to diminish the extracellular free DOX induced acute whole-body cytotoxicity, on the other hand it may circumvent the multidrug resistance associated with transporter provoked DOX effluxion *via* endocytic uptake pathway, thus compared to free DOX it is more suitable for clinical application.[50,51] The dual responsive magnetic nanocarriers are biocompatible for cells and are taken-up efficiently by two different cancer cell lines yet avoiding passive diffusion by efflux pumps through cell outer membrane.

Cytotoxicity of DOX vs MNC-DOXs in the absence of AMF

Cell cytotoxicity induced by different concentrations of DOX at three exposed durations (24 h, 48 h and 72 h) have been examined and compared between the DOX-MNCs and the free DOX through MTT cell viability assay for glioblastoma and breast carcinoma cell lines. The IC_{50} values (Table 2) for each condition has been determined and designated as the loading dose for the formulation in the following combination treatment, consequently. For both the cell lines, DOX concentration and incubation time dependent cytotoxicity effects were obtained for different exposure times (Figure 4). Comparison within the same cell line shows that the free DOX is much more cytotoxic than the DOX-MNCs. The IC_{50} values for encapsulated DOX group are nearly 10 times higher than the free ones on average. Especially for the breast cancer cell lines, the IC_{50} is even higher than 10 μg/mL. This lower cytotoxicity effect of the DOX-MNCs verified the previous results on the DOX and MNCs uptakes. As DOX molecules conjugated to the MNCs go through the endocytosis pathway that needs longer uptake time than the free DOX and without AMF stimulation, the majority of the drug still remained inside the endosomes or lysosomes with the nanocarriers, inducing subsequently less cytotoxicity as a result of less drug exposure to the nucleus.

AMF treatment of cancer cells loaded DOX-MNCs

Either a high concentration of chemotherapeutic drug or high temperature is powerful to kill the cancer cell alone. For the anticancer thermo-chemotherapy combination treatment, the evaluation of the synergistic effect, particularly at low doses is necessary for assessing therapeutic efficiency. For this purpose, our experiments have been performed at low concentration of DOX close to the IC_{50} value, i.e. 0.15 μg/mL for the U87 cell lines and 5.25 μg/mL for MCF-7 cell lines.

Table. 2 IC_{50} values of human glioblastoma U-87 cells and human breast adenocarcinoma MCF-7 cell lines after exposure with free DOX or DOX-MNCs for 24 h, 48 h and 72 h.

IC_{50} (μg/mL)	Cell line	Time (h)	24	48	72
	U-87	Free DOX	0.13	0.06	0.04
		DOX-MNCs	0.90	0.12	0.50
	MCF-7	Free DOX	0.95	0.29	0.16
		DOX-MNCs	>10	7.91	>10

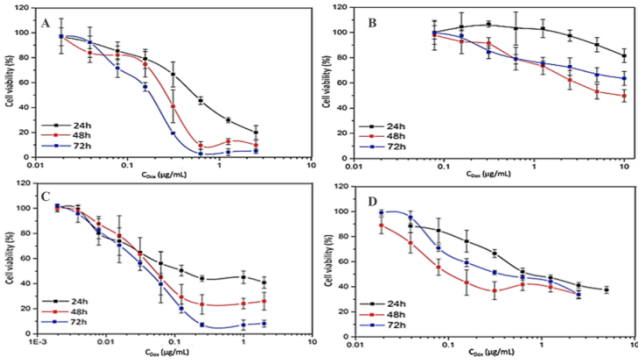


Figure 4. Dose response curves of human breast adenocarcinoma MCF-7 (A, B) and human glioblastoma U-87 cells (C, D) and incubated with DOX concentrations of either free DOX (A) (C) or DOX-MNCs (B) (D), all for 24 h, 48 h and 72 h.

As mentioned previously, inconsistent conclusion about additive or synergistic effects of combined thermo-chemotherapy concluded from the numerous publications suggested that different implementation approaches of hyperthermia might contribute to the overall therapeutic effect.[52] The extracellular and intracellular hyperthermia are

published version at https://doi.org/10.1039/D0TB01983F

Author manuscript version

Author manuscript version

the two most common approaches for magnetic fluid induced hyperthermia in literature, but they introduce the heat from totally different cellular locations.[26,53–55] In this study, extracellular heating involves subjecting the cells directly to the hyperthermia treatment immediately after mixing with the nanoparticles, thus applying heat only originating from the surrounding medium. The intracellular treatment was performed after 24 h internalization of 1 mg/mL suspension of nanoparticles with cells and subsequent washing of the extracellular nanoparticles. In this case, the heat is only generated by the nanoparticles internalized in endocytic components. Consequently, comparison of the synergistic effect between the two treatments in cancer cell lines could determine whether a heat treatment being released from the inside of the tumour cells or from the surrounding medium is more efficient for thermo-chemotherapy.

The internalized hyperthermia treatment has been performed under AMF with frequency 950 kHz and field amplitude 10.5 kA/m for 1 h. The cell viability at different time points after treatment was assayed with the Trypan Blue exclusion method. Although the previous publication has already verified that the AMF implementation does not affect cell viability.[55] In order to eliminate the unexpected variation, the cell AMF positive controls have been evaluated at 48 h time point in this study. The one-hour real-time heating curves indicate that the local temperature of the glioblastoma cell line U87 suspensions mainly retained at 39.2 °C, while the MCF7 cell suspensions stabilize at lower temperature 37.7 °C, due to the lower cellular uptake (See Suppl. 1). For both cell lines, the treatment procedure was below the normal mild hyperthermia temperature of 42 °C. Accordingly, the cell viability in the hyperthermia alone group only showed 20-30% reduction (Figure 5). Cellular viability decline within 48 h after one-shot of hyperthermia is consistent with the heat induced apoptosis pattern. [2,56] Notably, the U-87's cell viability has an increase trend from 72% to 79% within two days post-treatment incubation, which suggests that cells started recovering from insufficient thermal exposure. The ability of cancer recovery from under-estimated dose and even generating further thermal resistance also indicates the ongoing challenge about using hyperthermia alone in cancer treatment, as the complex tumour architecture and lack of reliable in site real-time temperature measurement made it nearly impossible to conduct a uniform and controlled heating dose among all the cancer cells.[55] Hence, a successful combinational treatment of hyperthermia and thermotherapy provides an important and significant improvement to current therapeutic strategy.

The result of our internalized combination treatment showed a statistically significant tumour cell suspension compared to the chemo treatment alone. The 48 h results are prominently promising as cell viability for U87 and MCF7 has been remarkably reduced to 4% and 11%, respectively. The combinational effectiveness has further been numerically assessed l by Valeriote's method (Table. 3).[57] Surprisingly, even at temperatures under the mild hyperthermia range, both cell lines have presented a synergistic effect of thermo-chemotherapy compared to thermo- or chemotherapy alone.

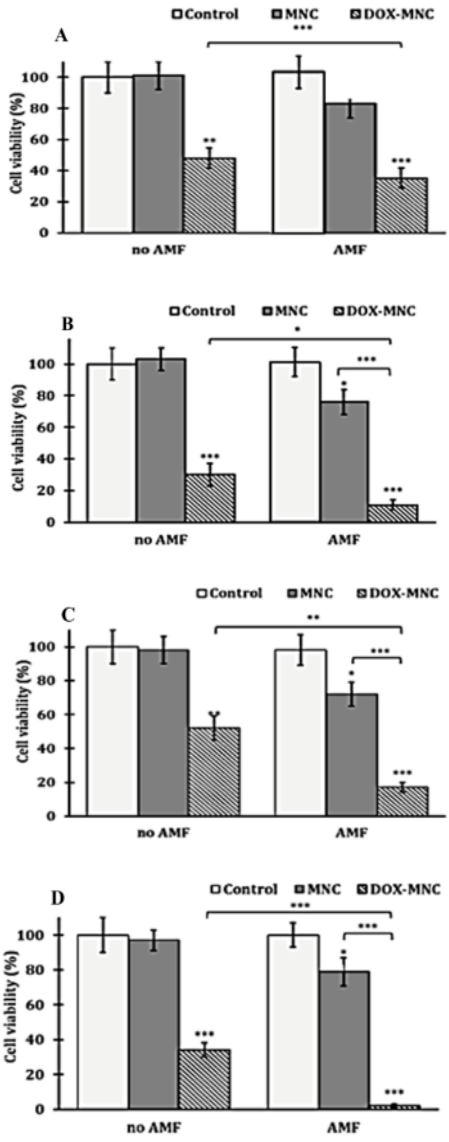


Figure 5. 24 h (A, C) and 48 h (B, D) post treatment cell viabilities of internalized nanoparticle hyperthermia for MCF-7 cells (A, B) and U-87 (C, D) after exposing with or without an AMF (1 h at *f* = 950 kHz and *H* = 10.5 kA/m) with media alone (control cells), MNCs or DOX-MNCs. The asterisks refer to significant levels compared to the corresponding control experiment or the combined therapy; $p < 0.05$ (*), $p < 0.01$ (**) and $p < 0.001$ (***).

published version at https://doi.org/10.1039/D0TB01983F

Author manuscript version

Author manuscript version

Table 3. Evaluation of the combined effect of the thermo (A)-chemo (B) therapy treatment on cell survival rate after nanoparticles internalization for both MCF-7 and U-87 cell lines according to Valeriote's formula.

	Time (h)	(A×B)/100 (%)	(A+B) (%)	Effect
MCF-7	24	40	35	Synergistic
	48	23	11	Synergistic
U-87	24	37	17	Synergistic
	48	27	2	Synergistic

Direct treatment of cancer cells with DOX-MNCs

The direct treatment of cells has been performed by identical hyperthermia protocol with the same dose of DOX but different amounts of MNCs. The same quantity of nanoparticles that got internalized by the cells after 24 h were incubated with the 1 mg/mL of nanoparticles, which is 75 µg per well has been used to compare with previous intracellular thermo-chemotherapy (Suppl. 2). Besides, direct treatment with 200 µg and 300 µg of MNCs were also used to assess if the higher temperature reached affects the effectiveness of the thermo-chemotherapy treatment.

The real-time heating curve of the cell suspensions at different MNC concentrations have been shown in Suppl. 2. The temperature of internalization equivalent to direct treatment group, 75 µg/mL, has reached a similar temperature to previous internalized magnetic hyperthermia treatment, 40 °C. The 200 µg/mL and 300 µg/mL groups approached to mild hyperthermia temperature 42 °C and 44 °C, respectively. Cell viability measured at 24 and 48 h after direct treatment for both hyperthermia alone and combination therapy exhibited a dramatic decline trend with regard to increased thermal dose for both cell lines (Figure 6): thermosensitivity is thus similar in both cell lines. It worth to mention an impressive cell elimination by the increased thermal does have been obtained in the hyperthermia alone group when the temperature reached 44 °C. The cell viability has dropped to 24% after 48 h post hyperthermia in MCF-7 cell lines and 26% in U-87 cell lines. This also indicates that an even higher temperature is required for hyperthermia alone**.** At each temperature, the combinational treatment demonstrated clear statistically significant superiority over individual treatment. The most potent combination result has been detected with the highest thermo-induced temperature, 44 °C as expected, in which the cell viability has decreased to 6% in MCF7 cell line and 15% in U-87 cell line. The synergistic efficiency that has been assessed via Valeriote's method was exhibited in Table 4.[57] Apart from the sub-additive effect of thermo-chemotherapy that was reported at 44 °C in U-87 cells and 42 °C in MCF-7 cells, the direct treatment of cancer cells with our drug delivery system have shown synergistic effects in all the other conditions. Furthermore, the maximum synergistic ratio of combination treatment has been observed at 40 °C in U-87 cell lines and 44 °C in MCF-7 cell lines, and the synergistic effect in U-87 cell lines was diminished by increasing magnetic hyperthermia temperature. The higher synergistic ratio at low temperature in specific cell line is of particular importance: if only a low hyperthermia temperature is needed for the treatment, the quantity of nanoparticles necessary for the treatment will remain low and achievable in the clinics, potentially achievable by intravenous injection instead of intra-tumoural as in the MagneTherm® protocol.

Table 4. Evaluation of the combined effects on cell survival rate of the direct thermo-chemotherapy treatment at different hyperthermia temperatures for MCF-7 and U-87 cell line according to Valeriote's formula.

		Time (h)	(A)×(B)/100 (%)	(A+B) (%)	Effect
MCF-7	40 °C	24	55	53	Synergistic
		48	32	28	Synergistic
	42 °C	24	46	47	Sub-additive
		48	25	30	Sub-additive
	44 °C	24	27	14	Synergistic
		48	11	6	Synergistic

		Time (h)	(A)×(B)/100 (%)	(A+B) (%)	Effect
U-87	40 °C	24	59	42	Synergistic
		48	35	25	Synergistic
	42 °C	24	42	40	Synergistic
		48	23	21	Synergistic
	44 °C	24	27	32	Sub-additive
		48	12	15	Sub-additive

published version at https://doi.org/10.1039/D0TB01983F

Author manuscript version

Author manuscript version

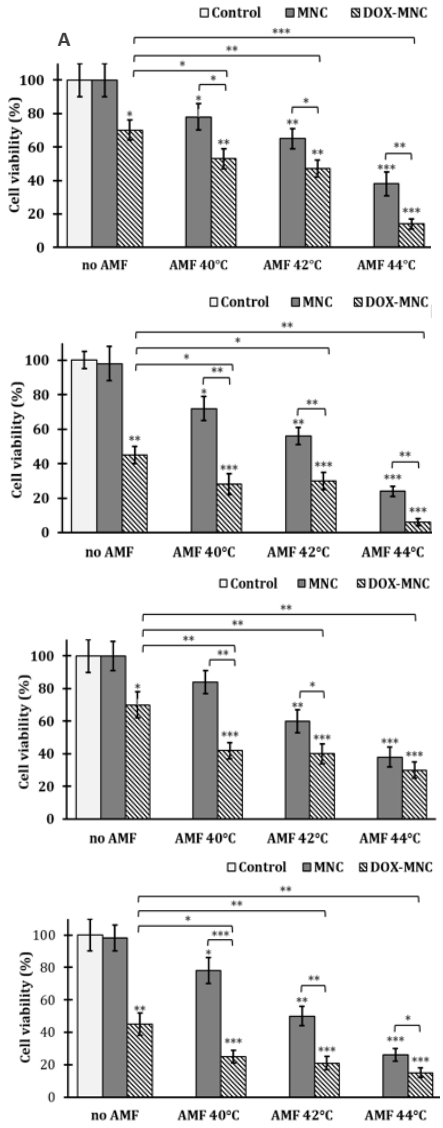


Figure 6. 24 h (A, C) and 48 h (B, D) post treatment cell viabilities of direct hyperthermia for MCF-7 (A, B) cells and U-87 (C, D) following direct treatment with or without a 1 h exposure to an AMF (f = 950 kHz and H = 10.5 kA/m) with media control or contain MNCs or DOX-MNCs. The asterisks refer to significant levels compared to the corresponding control experiment or the combined therapy; $p < 0.05$ (*), $p < 0.01$ (**) and $p < 0.001$ (***).

These results imply that different thermal doses could lead to distinctive thermo-chemosensitisation effects in particular cell lines, which emphasizes the importance of an appropriate thermal dose in designating direct thermo-chemotherapy for individual cell lines. The mechanisms behind this phenomenon may be contributed by the different behaviours driven from different cell lines and non-linear thermal induced cellular uptake of chemodrugs.[58] In the direct treatment, there was not enough time for nanoparticles to be up-taken by the cells, which means unlike internalized modality most of the antineoplastic drugs were only released by heating outside of the cells.

Although the increased cell membrane permeability associated with promoting drugs accumulation into tumour cells by raising temperature have been proved,[59] some publications demonstrated, for DOX, that a prominent increase of intracellular accumulation reported with 40 °C hyperthermia but was not observed at 43 °C, *in vivo*.[60,61] This result corroborates our finding of sub-additive effects observed at 44 °C in the case of U-87 cells. Direct treatment (*i.e.* extracellular) of cancer cells with DOX-MNCs shows either synergistic or sub-additive effect.

Synergistic effect of DOX-MNCs on the RM1-CMV-LucF cells

The promising synergistic results of DOX-MNC induced thermo-chemotherapy on both MCF-7 and U-87 human cell lines have revealed the potential to apply this system to other cell lines. However, the thermosensitisation differences between that of two cell lines also highlight the importance of elaborative analysis of particular cell lines before application. Moreover, the previous evaluation was based on the trypan blue dye exclusion assay, which may underestimate the therapeutic efficiency by excluding the cells that undergo an early disintegration. Thus, the combinational treatment of our system in genetically modified murine prostate cancer cell line RM1-CMV-LucF has been tested *via* a bioluminescence imaging (BLI) assay.[62] Cytotoxicity effects of DOX-MNC alone and of combination of intracellular and extracellular hyperthermia treatments were examined by monitoring their luciferase expression, which is correlated to cell metabolic activity, through the BLI method.

The dose-response curve of cytotoxicity of DOX-MNCs after 24 h and 48 h incubation is illustrated on Figure 7. It shows an increasing cytotoxicity with higher DOX concentration or longer incubation time. The IC_{50} values after 24 h and 48 h of incubation were found to be equivalent to a DOX concentration of 2.12 µg/mL and 0.16 µg/mL, respectively. According to this, a low DOX concentration of 0.18 µg/mL in the subsequent experiments have been used to analyse the synergistic effect. As the preliminary tests have shown 42 °C was more efficient for the combined therapy than hyperthermia at 40 °C or 44 °C for this specific cell line, the hyperthermia temperatures of 42 °C and 43 °C were studied in the direct treatment. During the 30 min hyperthermia under the AMF with f = 217 kHz and H = 20 kA/m, the temperature has been adjusted and maintained by tuning the field amplitude H along the AMF application. The outcome of either intracellular hyperthermia or extracellular hyperthermia exhibited the similar decreasing pattern with the previous MCF-7 and U-87 cell lines (Figure 8). The cytotoxic effect of the combinatorial treatment achieved with the developed nanodrug delivery system was found statistically superior to either hyperthermia or chemotherapy applied separately. This satisfactory synergistically effect of the thermo-chemotherapy for both hyperthermia proceeding methods has been evaluated numerically by Valeriote's formula in Tab 5. Notability, the cell viability of hyperthermia treatment alone after internalization reached as low as 65%, which is a drastically higher

published version at https://doi.org/10.1039/D0TB01983F

Author manuscript version

Author manuscript version

toxic effect than the 89% at 42 °C and 71% at 43 °C in direct treatment. This noticeable viability reduction by internal hyperthermia has not been observed in the other two cell lines, which suggests that RM1-CMV-LucF cell lines may be more sensitive to the heat released from intracellular nanoparticles.

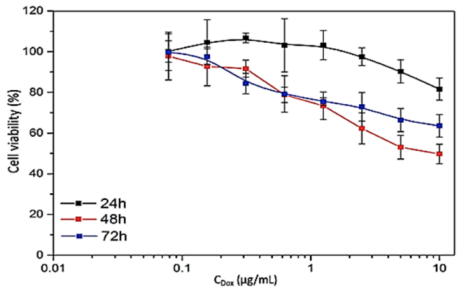


Figure 7. Dose response curves of RM1-CMV-LucF cells incubated with DOX-MNCs in the series of dilutions according to DOX concentration for 24 h and 48 h incubation.

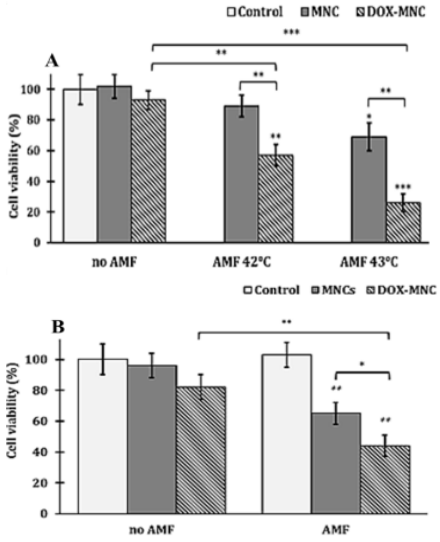


Figure 8. Cell viabilities of RM1-CMV-LucF cells 24 h following either (A) direct treatment and (B) treatment after internalization. The asterisks refer to significant levels compared to the corresponding control experiment or the combined therapy; $p < 0.05$ (*), $p < 0.01$ (**) and $p < 0.001$ (***).

Table 5. Evaluation of the combined effects of the thermo-chemotherapy treatment after nanoparticle internalization or direct thermo-chemotherapy treatment at different hyperthermia temperatures for RM1-CMV-LucF cell line according to Valeriote's formula. In case of intracellular hyperthermia, temperature did not increase under AMF application (i.e. it remained 37 °C).

		(A)×(B)/100 (%)	(A+B) (%)	Effect
Intracellular treatment		53	44	Synergistic
Extracellular treatment	42 °C	83	59	Synergistic
	43 °C	64	27	Synergistic

Comparison between the intracellular and extracellular hyperthermia in combination therapy in all three cell lines have highlighted that the method of conducting magnetic hyperthermia greatly influences the combination therapy results. No matter whether a cell line have internalized the desired nanoparticles in a high amount, such as the U-87 cells, or not, like MCF-7 cell lines, the intracellular hyperthermia induced a better thermo-chemotherapy synergistic result than the extracellular treatment method (Tables 3, 4, 5). Remarkably, in the high nanoparticle uptake U-87 cell line, the cell viabilities for the combined therapy in intracellular heating group reached values as low as 17% and 2%, 24 h and 48 h after the treatment, respectively. The results were not only lower than the equilibrated direct therapeutic group: 40% and 25%, but also, more pronounced than the best outcomes achieved in direct hyperthermia group: 32% and 15%. Although a promising thermo-chemotherapy result has been accomplished in all cells with both hypothermia methods, the finding demonstrates that it is more effective therapy if tumour cells internalise the nanoparticles.

Experimental

Materials

Materials for nanocarrier synthesis: Iron (II) chloride tetrahydrate, iron (III) chloride hexahydrate, sodium carbonate, hydrochloric acid, poly(ethylene glycol) methyl ether methacrylat，di(ethylene glycol) methyl ether methacrylate, 3-(trimethoxysilyl)propyl methacrylate, 3-vinylbenzaldehyde, 4,4-azobis(4-cyanovaleric acid), 4-cyano-4-(phenylcarbonothioylthio)-pentatonic acid, chloroform-d NMR solvent, triethylamine, acetonitrile, toluene, and petroleum ether were purchased from Sigma-Aldrich, UK. Tetrahydrofuran was provided from Wako chemicals, UK.

Materials for biology experiments: 0.4% trypan blue solution, dimethyl sulfoxide (DMSO, purity ≥ 99.9%), hydrochloric acid (HCl, 37 wt.%), hexacyanoferrate trihydrate ($K_4Fe(CN)_6{\cdot}3H_2O$), nuclear fast red (0.1%, w/v), accutase solution and minimum essential cell growth medium eagle (MEM) were purchased

published version at https://doi.org/10.1039/D0TB01983F

Author manuscript version

Author manuscript version

from Sigma-Aldrich, UK. 3-(4,5-Dimethyl-2-thiazolyl)-2,5-diphenyl-2H-tetrazolium bromide (thiazolyl blue tetrazolium bromide MTT, 98%) was obtained from Alfa Aesar, UK. Ethanol (100%) was obtained from Hayman, UK. The other chemicals and mediums were acquired from Gibco Thermo Fisher scientific, UK. All sterile reagents were used as purchased without any further modification; the rest were sterile filtered to avoid any contamination in the biology procedure.

Synthesis of doxorubicin loaded magnetic nanocarrier

The superparamagnetic nanoparticle cores in this nanocarrier were first synthesized *via* modified co-precipitation method with the aid of microwave reactor (CEM Discover SP).[63,32] Then the P(DEGMA-*co*-PEGMA-*b*-[TMSPMA-co-VBA]) polymer, which was synthesized by adjusted reversible addition-fragmentation chain transfer (RAFT) polymerization, were grafted to the nanoparticle surfaces through the silanisation reaction between the hydroxyl groups of the bare magnetic nanoparticle and the trimethoxysilane groups of the polymer.[64] Finally, the doxorubicin was conjugated to the MNCs though formation of pH-cleavable Schiff base bonds.[64,32] Full characterisation has been performed to control the quality of the nanocarriers before their use in biological experiments.

Cell Culture

U87-MG glioblastoma cell line, mouse fibroblast cell line L929 and genetic modified Luciferase firefly (LucF) expressed murine prostate carcinoma cell line RM1-CMV-LucF were cultured in Dulbecco's modified eagles medium (DMEM), while MCF7 breast cancer cell line was cultured in MEM. All complete medium was supplemented with 10% foetal bovine serum (FBS), 1% penicillin/streptomycin and 1% L-glutaMAX. The cells were cultured at 37 °C under 5% CO_2 in humidity stable incubators. They were detached at approximately 80%-90% confluence by trypsinization for the further experiments.

Intracellular internalization imaging

In order to identity the intracellular internalization of MNCs. The Prussian blue (PB) staining assay was used to visualize the iron oxide core. Fluorescence microscopy was employed to track the DOX in cells from its red emission.

Prussian blue histology staining: Prior to both visualizations, MCF-7 and U87 cells were grown on coverslips at the density of 5.0×10^4 cells/well inside 24 well plates for 72 h to reach confluence. Then for the Prussian blue histology staining, the cell culture was substituted by MNCs suspension medium with different concentration: 1 mg/mL, 0.5 mg/mL, 0.1 mg/mL, 0.05 mg/mL, 0.01 mg/mL and 0.00 mg/mL for 4 h or 24 h to allow the particle internalization. Followed by three times complete medium and twice Dulbecco's phosphate-buffered saline (DPBS) washings, cells were fixed with 4% paraformaldehyde for 30 min at room temperature. Afterwards, the cells were stained by fresh prepared Prussian blue solution for 2 min and counterstained with nuclear fast red for another 2 min. Finally, the cells were dehydrated with alcohol and mounted onto microscope glass slides for fluorescence imaging on an inverted optical microscope (DMI600B, Leica, UK).

Fluorescence microscopy: After cell confluence, the culture medium was replaced by the 1 ml of medium that containing either DOX solution or DOX-MNCs with an equivalent amount of 4 µg DOX for 3 h or 24 h. Then the free DOX or nanocarriers were fully removed by four times medium and twice DPBS washing. After 30 min 4% paraformaldehyde fixation, the cell was rinsed twice again with DPBS before it stained with 5 µM nuclear dye, DRAQ5 for 15 min in the dark. The coverslips were rinsed with Milli-Q water and mounted in a slide using Fluor Preserve mounting medium before observation with microscope (DMI600B, Leica, UK). The excitation wavelength 488 nm was used for both DOX and DRAQ5. The fluorescence emissions of these two were observed by a rhodamine (N3 ET, 600/40 bandpass filter, Leica) and a far-red (Y5 ET, 700/75 bandpass filter, Leica) filter sets, respectively. Images were captured using LAS X software.

Quantification of intracellular iron content

The SQUID magnetometer (PPMS, Quantum Device™) was used to quantify the MNCs content in MCF7 and U87 cell lines. The cells were cultured in 12 well plates at 1.0×10^5 cells/well seeding density for 72 h, then treated with different concentrations of MNCs containing medium (i.e. 1 mg/mL, 0.5 mg/mL, 0.1 mg/mL, 0.05 mg/mL, 0.01 mg/mL and 0.00 mg/mL) for 4 or 24 h to allow the internalization of the MNCs. After gently removing of the free nanoparticles by washing three times in medium and twice in DPBS too, the cells were collected by trypsinization and centrifugation. The total cell number was estimated by calculating the cell density of 0.5 mL re-suspending cell pellet medium via haemocytometer. Then, the cell pellets were collected by centrifugation again and transferred into powder polycarbonate sample holder for SQUID-VSM. Samples were dried in a low temperature oven at 37 °C overnight before carrying out the magnetic measurements.

Cytotoxicity and cell viability assays

MTT assay: After incubation and treatment, the MTT solution was added to every well to a final concentration of 200 µg/mL incomplete cell culture medium for 4 h. Then, the MTT contained medium was discarded and fixed amount of DMSO was added into the wells to dissolve the formazan crystals. The proportion of viable cells was calculated by absorbance measured on a microplate reader (VersaMax™, Molecular Devices, USA) at 540 nm.

published version at https://doi.org/10.1039/D0TB01983F

Author manuscript version

Author manuscript version

Trypan blue dye exclusion assay: Cells from each treatment group were trypsinized with 0.4 mL trypsin and dispersed in 1 mL of fresh media. 50 µL of cell suspension was stained with equal amount of sterile-filtered trypan blue then counted by a haemocytometer. The viability of treated group was calculated relatively to the corresponding control.

Bioluminescence assay: Briefly, at the end of incubation the medium was removed from RM1-CMV-LucF cell cultures before washing with DPBS. D-luciferin was added at 6.10^{-4} M bioluminescence image was captured 5 min later on an IVIS Lumina™ LT (Perkin Elmer Inc., USA) and analysed by Living Image® software. The percentage of viable cells for each group was expressed as a percentage of the vehicle control.

Biocompatibility evaluation

L929 cells were plated in 96 well plates at a concentration of 1.0×10^3 cells/well for 72 h. Then 100 µL of medium in each well was replaced by different concentrations of MNCs containing medium, from 0 to 1 mg/mL, and incubated for another 48 h. Finally, the cell viability was calculated by the MTT assay.

Cytotoxicity Comparison

In order to evaluate the cytotoxicity difference between free DOX and DOX-MNCs at different exposure times among cell lines and to provide the potency baseline for the following combination treatment assays, the IC_{50} was been calculated via CompuSyn® software.

The IC_{50} determination for MCF7 and U87 cell lines: cells were plated in 96 well plates at a concentration of 5.0×10^3 cells/well. After 24 h, different concentrations of medium that contain either free DOX or DOX-MNCS were added into the cells for another 24, 48 or 72 h. High concentration DOX stock was diluted in DMSO. Control wells contained the same amount of DMSO, to normalize the cell cytotoxicity coming from the vehicle. MTT assay was performed as previously described.

RM1-CMV-LucF cell line: Cells were plated at 2.5×10^4 cells/well density in 24 well plates for 48 h before growing in different concentration of either free DOX or DOX-MNCS contained medium for another 24 h and 48 h. After that, the cell viability was calculated based on the photons counts in region of interest (ROI) placed on bioluminescence images of each wells.

Treatment protocol for thermo-chemotherapy evaluation

In order to evaluate the synergetic effect of magnetic nanoparticle in the combination treatment over hyperthermia itself *in vitro*, both direct and internalized hyperthermia protocols have been conducted for all cell lines. In each set of experiments, the cultured cell has been grouped as followed: Control, treated with MNCs and DOX-MNCs groups. Half of them have gone through AMF induced hyperthermia, and the rest stayed as control. Hyperthermia groups: control+ (media only, AMF), MNCs+ (media containing MNCs, AMF) and DOX-MNCs+ (media containing DOX-MNCs, AMF). Hyperthermia control groups: Control (media only, no AMF), MNCs- (media containing MNCs, no AMF) and DOX-MNCs- (media containing DOX-MNCs, no AMF). The effect of the combination efficient was evaluated by Valeriote's method as following:

- synergistic: $(A + B) < (A) \times (B)/100$
- additive: $(A + B) = (A) \times (B)/100$
- sub-additive: $(A) \times (B)/100 < (A + B) < (A)$ if $(A) < (B)$
- interference: $(A) < (A + B) < (B)$, if $(A) < (B)$
- antagonistic: $(B) < (A + B)$, if $(A) < (B)$.

A and B stand for the cell viability for hyperthermia and chemotherapy respectively.

Intracellular thermo-chemotherapy

MCF7 and U87 cell lines: The seeding density for 12 well plates are 1.5×10^5 cells/well. After 24 h pre-incubation, MNCs or DOX-MNCs at a concentration of 1 mg/mL of Fe and 0.15 µg/mL of DOX were added into the cells for 24 h to allow their full internalization. Subsequently the free nanoparticles were washed away and the cells from each group were collected and redisposed in 0.5 mL medium before applying hyperthermia under an AMF H = 10.5 kA/m and f = 950 kHz for 1 h using a MACH instrument (Resonant Circuits Limited, London, UK). After treatment, cells were seeded in 12 well plates and their viability were analysed after 24 or 48 h *via* the trypan blue dye exclusion assay.

For RM1-CMV-LucF cell line: 1.0×10^5 cells were grown in 3 mL of medium in every 35 mm culture dishes for 48 h before being treated with fresh media or the media that contained 1 mg/mL of iron containing MNCs or DOX-MNCs. Then the free MNCs and DOX-MNCs were washed away from cells after 24 h internalization. The 3 AMF positive groups were exposed to H = 20.0 kA/m and f = 217 kHz magnetic field for 30 min using the DM3 instrument (Nanoscale Biomagnetics™, Zaragoza, Spain). The AMF negative groups were subjected to the same protocol without being treated by magnetic hyperthermia. After the 30 min treatment, the cells were incubated for 24 h before measuring the cell viability by the BLI measurement method.

2.11. Extracellular thermo-chemotherapy. MCF7 and U87 cell lines: The same protocols as for the after-internalization method was used, apart from the nanoparticles for direct heating were added only right before the exposure of the cells to hyperthermia treatment. Briefly, after collecting the cell pellet, 0.5 mL of fresh media or MNCs or DOX-MNCs contained medium were transferred into a vial for hyperthermia treatment. The DOX in all nanocarrier groups was 0.15 µg/mL that is same as treatment after internalization protocol. Iron concentration of 75 µg/mL was used for the hyperthermia treatment at 40 °C, which was equal to the nanoparticle concentration internalized after exposure of U-87 cells for 24 h

published version at https://doi.org/10.1039/D0TB01983F

Author manuscript version

Author manuscript version

with a solution of 1 mg/mL of MNCs. Concentrations of 200 µg/mL and 300 µg/mL were used for the hyperthermia treatment at 42 °C and 44 °C, respectively. After this, identical treatments and analysis procedures were used as mentioned in the internalization hyperthermia protocol.

Test for RM1-CMV-LucF cell line

2000 cells suspended in 200 µL medium were seeded in 16-well plates for 48 h before transfer in media that contained or without nanoparticles. The iron concentration for both MNCs and DOX-MNCs was reduced to 0.5 mg/mL but the DOX concentration was the same as in the previous internalizing RM1 cell lines hyperthermia protocol. The cells of positive groups were treated 30 min under the AMF field (f = 217 kHz) at either 42 °C or 43 °C. The temperature was adjusted by tuning the field amplitude H of the AMF. After that, the following steps were the same as mentioned before.

Statistical analysis

In order to acquire significant results, all experiments were accomplished in triplicate. Statistical analysis was performed using the Student's t-test for unpaired data and the results are presented as mean ± standard deviations. Statistical significance was accepted at a level of $p < 0.05$.

Conclusions

In our previous paper, the excellent chemical and physical performances of a successful constructed dual response drug nanocarrier have already been demonstrated but only *ex vitro* and without AMF application. Therefore, this comprehensive biological study further establishes the biocompatibility and the therapeutic efficiency of our system under applied AFM *in vitro*, which will guide the further translation steps into medical application, first through preclinical assays on animals. The MNCs used were found to be biocompatible and efficient as nanoheaters even for concentrations as low as 1 mg/mL. A significant variation of MNCs cellular uptake between different cell lines has been demonstrated *via* multiple techniques. Besides, the previous publication prediction was based on the *ex vitro* simulative drug releasing profiles only. Here the DOX-MNCs have been revealed to be taken up through endocytosis and to capture a considerable DOX amount within the cytoplasm, without further macroscopic heating stimulation, which results in slow DOX delivery to the nuclei. This affected both the DOX-MNCs induced cytotoxicity and the combination therapy effects for these cell lines. More specifically, this dual response system limited the cellular and systemic cytotoxicity compared to free DOX without AMF stimulation, enabling the lower side-effect when the therapy is applied *in vivo*. The thermo-chemotherapy treatment implemented with our system presented a much more potent and synergistic effect than that of either chemotherapy or magnetic hypothermia alone, for multi-modal cancer therapy in nearly every studied condition. An almost complete cell death was observed for U-87 and MCF-7 cell lines. Moreover, our study demonstrated for the first time a detailed comparison of magnetic nanoparticle stimulated thermo-chemotherapy between intercellular and extracellular heating in multiple cell lines. The results indicated that each cell lines have different behaviours and responses from one another to the deposited thermal dose and heating application pathway in the combination treatment, which highlights the necessity to study each cell line independently for a given treatment. These promising *in vitro* results confirm that the successful development of DOX-loaded dual pH- and thermo-responsive magnetic nanocarriers constitutes a step forward towards design of the next generation of nanosystems that are envisioned for future *in vivo* and clinical applications.

Conflicts of interest

There are no conflicts to declare.

Acknowledgements

NTKT thanks EPSRC (EP/M015157/1 and EP/M018016/1); AOARD (FA2386-17-1-4042 award) and European COST action TD1402 RadioMag for funding. AH was supported by UCL-JAIST PhD program. This study was achieved within the context of the Laboratory of Excellence TRAIL ANR-10-LABX-57. Dr Florian Aubrit is acknowledged for contributing to the drawing of the journal cover artwork.

Notes and references

1 R. D. Issels, *Eur. J. Cancer*, 2008, **44**, 2546–2554.
2 M. W. Dewhirst, B. L. Viglianti, M. Lora-Michiels, M. Hanson and P. J. Hoopes, *Int. J. Hyperth.*, 2003, **19**, 267–294.
3 P. Prakasa Babu, Y. Yoshida, M. Su, M. Segura, S. Kawamura and N. Yasui, *Neurosci. Lett.*, 2000, **291**, 196–200.
4 J. Yoo, H. R. C. Kim and Y. J. Lee, *Int. J. Hyperth.*, 2006, **22**, 713.
5 P. Clerc, P. Jeanjean, N. Hallalli, M. Gougeon, B. Pipy, J. Carrey, D. Fourmy and V. Gigoux, *J. Control. Release*, 2018, **270**, 120–134.
6 A. Dieing, O. Ahlers, B. Hildebrandt, T. Kerner, I. Tamm, K. Possinger and P. Wust, *Prog. Brain Res.*, 2007, **162**, 137–152.
7 V. J. Verwaal, S. Bruin, H. Boot, G. Van Slooten and H. Van Tinteren, *Ann. Surg. Oncol.*, 2008, **15**, 2426–2432.
8 D. M. Katschinski, G. J. Wiedemann, W. Longo, F. R. D'Oleire, D. Spriggs and H. I. Robins, *Cytokine Growth Factor Rev.*, 1999, 10, 93–97.
9 Y. Harima, K. Nagata, K. Harima, V. V Ostapenko, Y. Tanaka and S. Sawada, *Int. J. Hyperth.*, 2009, **25**, 338–343.
10 H. I. Robins, J. D. Cohen, C. L. Schmitt, K. D. Tutsch, C. Feierabend, R. Z. Arzoomanian, D. Alberti, F. D'Oleire, W. Longo, C. Heiss, D. Rushing, R. Love and D. Spriggs, *J. Clin. Oncol.*, 1993, **11**, 1787–1794.
11 P. Wust, B. Hildebrandt, G. Sreenivasa, B. Rau, J. Gellermann, H. Riess, R. Felix and P. Schlag, *Lancet Oncol.*, 2002, **3**, 487–497.
12 Z. X. Wang, B. Zhang, S. M. Deng and S. J. Chen, *Chin. Med. J. (Engl).*, 2012, **125**, 657–661.
13 G. J. Wiedemann, E. Knop, M. Mentzel, J. Geisler, T. Wagner, S. Eleftheriadis, P. Schmucker, M. Klouche, T. Feyerabend, C. Weiss, S. Feddersen, P. Bucsky and F. D'Oleire, *Cancer Res.*, 1994, **54**, 5346–5350.

Author manuscript version

Author manuscript version

14 G. Helmlinger, F. Yuan, M. Dellian and R. K. Jain, *Nat. Med.*, 1997, **3**, 177–182.
15 B. Hildebrandt, P. Wust, O. Ahlers, A. Dieing, G. Sreenivasa, T. Kerner, R. Felix and H. Riess, *Crit. Rev. Oncol. Hematol.*, 2002, **43**, 33–56.
16 H. Maeda, J. Wu, T. Sawa, Y. Matsumura and K. Hori, *J. Control. Release*, 2000, **65**, 271–284.
17 H. Maeda, *J. Control. Release*, 2012, **164**, 138–144.
18 I. Hilger, *Int. J. Hyperth.*, 2013, **29**, 828–834.
19 S. T. Heijkoop, H. C. van Doorn, L. J. a Stalpers, I. a Boere, J. van der Velden, M. Franckena and A. M. Westermann, *Int. J. Hyperthermia*, 2013, **6736**, 1–5.
20 R. K. Gilchrist, R. Medal, W. D. Shorey, R. C. Hanselman, J. C. Parrott and C. B. Taylor, *Ann. Surg.*, 1957, **146**, 596–606.
21 K. Maier-Hauff, R. Rothe, R. Scholz, U. Gneveckow, P. Wust, B. Thiesen, A. Feussner, A. von Deimling, N. Waldoefner, R. Felix and A. Jordan, *J. Neurooncol.*, 2007, **81**, 53–60.
22 M. Johannsen, U. Gneveckow, K. Taymoorian, B. Thiesen, N. Waldöfner, R. Scholz, K. Jung, A. Jordan, P. Wust and S. A. Loening, *Int. J. Hyperth.*, 2007, **23**, 315–323.
23 Z. Hedayatnasab, F. Abnisa and W. M. A. W. Daud, *Mater. Des.*, 2017, **123**, 174–196.
24 J. Kolosnjaj-Tabi, R. Di Corato, L. Lartigue, I. Marangon, P. Guardia, A. K. A. Silva, N. Luciani, O. Clément, P. Flaud, J. V. Singh, P. Decuzzi, T. Pellegrino, C. Wilhelm and F. Gazeau, *ACS Nano*, 2014, **8**, 4268–4283.
25 R. T. Gordon, J. R. Hines and D. Gordon, *Med. Hypotheses*, 1979, **5**, 83–102.
26 A. Jordan, R. Scholz, P. Wust, H. Schirra, Thomas Schiestel, H. Schmidt and R. Felix, *J. Magn. Magn. Mater.*, 1999, **194**, 185–196.
27 A. Jordan, R. Scholz, K. Maier-Hauff, M. Johannsen, P. Wust, J. Nadobny, H. Schirra, H. Schmidt, S. Deger, S. Loening, W. Lanksch and R. Felix, *J. Magn. Magn. Mater.*, 2001, **225**, 118–126.
28 C. Blanco-Andujar, D. Ortega, P. Southern, S. A. Nesbitt and N. T. K. Thanh, *Nanomedicine*, 2016, **11**, 121–136.
29 V. T. A. Nguyen, M. C. De Pauw-Gillet, M. Gauthier and O. Sandre, *Nanomaterials*, 2018, **8**, 1014.
30 P. Moroz, S. K. Jones and B. N. Gray, *Int. J. Hyperth.*, 2002, **18**, 267–284.
31 Y. Rabin, *Int. J. Hyperth.*, 2002, **18**, 194–202.
32 A. Hervault, A. E. Dunn, M. Lim, C. Boyer, D. Mott, S. Maenosono and N. T. K. Thanh, *Nanoscale*, 2016, **8**, 12152–12161.
33 S. V. Spirou, S. A. Costa Lima, P. Bouziotis, S. Vranješ-Djurić, E. K. Efthimiadou, A. Laurenzana, A. I. Barbosa, I. Garcia-Alonso, C. Jones, D. Jankovic and O. L. Gobbo, *Nanomaterials*, 2018, **8**, 306.
34 S. Naahidi, M. Jafari, F. Edalat, K. Raymond, A. Khademhosseini and P. Chen, *J. Control. Release*, 2013, **166**, 182–194.
35 I. Fratoddi, *Nanomaterials*, 2018, **8**, 1–23.
36 X. Li, L. Wang, Y. Fan, Q. Feng and F. Z. Cui, *J. Nanomater.*, 2012, 2012, 1–19.
37 R. Gref, A. Domb, P. Quellec, T. Blunkc, R. H. Müllerd, J. M. Verbavatze and and R. Langer, *Bone*, 1995, **23**, 1–7.
38 G. Zhang, Z. Yang, W. Lu, R. Zhang, Q. Huang, M. Tian, L. Li, D. Liang and C. Li, *Biomaterials*, 2009, **30**, 1928–1936.
39 D. E. Owens and N. A. Peppas, *Int. J. Pharm.*, 2006, 307, 93–102.
40 G. Hemery, C. Genevois, F. Couillaud, S. Lacomme, E. Gontier, E. Ibarboure, S. Lecommandoux, E. Garanger and O. Sandre, *Mol. Syst. Des. Eng.*, 2017, **2**, 629–639.
41 John L. Nitiss, *NIH Public Access*, 2009, **9**, 1–27.
42 C. F. Thorn, C. Oshiro, S. Marsh, T. Hernandez-Boussard, H. McLeod, T. E. Klein and R. B. Altman, *Pharmacogenet. Genomics*, 2011, **21**, 440–446.
43 Z. Zhao, D. Huang, Z. Yin, X. Chi, X. Wang and J. Gao, *J. Mater. Chem.*, 2012, **22**, 15717–15725.
44 K. K. Upadhyay, A. N. Bhatt, A. K. Mishra, B. S. Dwarakanath, S. Jain, C. Schatz, J. F. Le Meins, A. Farooque, G. Chandraiah, A. K. Jain, A. Misra and S. Lecommandoux, *Biomaterials*, 2010, **31**, 2882–2892.
45 O. Taratula, R. K. Dani, C. Schumann, H. Xu, A. Wang, H. Song, P. Dhagat and O. Taratula, *Int. J. Pharm.*, 2013, **458**, 169–180.
46 A. D. Heibein, B. Guo, J. A. Sprowl, D. A. MacLean and A. M. Parissenti, *BMC Cancer*, 2012, **12**, 1–14.
47 J. White, A. Helenius and M. J. Gething, *Nature*, 1982, **300**, 658–659.
48 S. Zhang, H. Gao and G. Bao, *ACS Nano*, 2015, **9**, 8655–8671.
49 G. Sahay, D. Y. Alakhova and A. V. Kabanov, *J. Control. Release*, 2010, **145**, 182–195.
50 S. Aluri, S. M. Janib and J. A. Mackay, *Adv. Drug Deliv. Rev.*, 2009, **61**, 940–952.
51 M. Shi, K. Ho, A. Keating and M. S. Shoichet, *Adv. Funct. Mater.*, 2009, **19**, 1689–1696.
52 A. Hervault and N. T. K. Thanh, *Nanoscale*, 2014, **6**, 11553–11573.
53 K. Fang, L. Song, Z. Gu, F. Yang, Y. Zhang and N. Gu, *Colloids Surfaces B Biointerfaces*, 2015, **136**, 712–720.
54 M. L. Mojica Pisciotti, E. Lima, M. Vasquez Mansilla, V. E. Tognoli, H. E. Troiani, A. A. Pasa, T. B. Creczynski-Pasa, A. H. Silva, P. Gurman, L. Colombo, G. F. Goya, A. Lamagna and R. D. Zysler, *J. Biomed. Mater. Res. - Part B Appl. Biomater.*, 2014, **102**, 860–868.
55 C. Blanco-Andujar, D. Ortega, P. Southern, S. A. Nesbitt, N. T. K. Thanh and Q. A. Pankhurst, *Nanomedicine*, 2016, **11**, 121–136.
56 M. Yonezawa, T. Otsuka, N. Matsui, H. Tsuji, K. H. Kato, A. Moriyama and T. Kato, *Int. J. Cancer*, 1996, **66**, 347–351.
57 F. Valeriote and H. Lin, *Cancer Chemother. reports*, 1975, **59**, 895—900.
58 F. Mohamed, P. Marchettini, O. A. Stuart, M. Urano and P. H. Sugarbaker, *Ann. Surg. Oncol.*, 2003, **10**, 463–468.
59 J. P. May and S. D. Li, *Expert Opin. Drug Deliv.*, 2013, **10**, 511–527.
60 M. Peller, L. Willerding, S. Limmer, M. Hossann, O. Dietrich, M. Ingrisch, R. Sroka and L. H. Lindner, *J. Control. Release*, 2016, **237**, 138–146.
61 S. Nagaoka, S. Kawasaki, Y. Karino, Y. Hiraki and T. Nakanishi, *J. Radiat. Res.*, 1987, **28**, 262–267.
62 L. Adumeau, C. Genevois, L. Roudier, C. Schatz, F. Couillaud and S. Mornet, *Biochim. Biophys. Acta - Gen. Subj.*, 2017, **1861**, 1587–1596.
63 C. Blanco-Andujar, D. Ortega, P. Southern, Q. A. Pankhurst and N. T. K. Thanh, *Nanoscale*, 2015, **7**, 1768–1775.
64 A. E. Dunn, D. J. Dunn, A. Macmillan, R. Whan, T. Stait-Gardner, W. S. Price, M. Lim and C. Boyer, *Polym. Chem.*, 2014, **5**, 3311–3315.

published version at https://doi.org/10.1039/D0TB01983F

Author manuscript version

In vitro exploration of the synergistic effect of alternating magnetic field mediated thermo-chemotherapy with doxorubicin loaded dual pH- and thermo-responsive magnetic nanocomposite carriers

Lilin Wang,[a,b] Aziliz Hervault,[a,b,] Paul Southern,[b,c] Olivier Sandre,[e] Franck Couillaud[d] and Nguyen Thi Kim Thanh[a,b,*]

[a.] *Biophysics Group, Department of Physics &Astronomy, University College London, Gower Street, London, WC1E 6BT, UK.*

[b.] *UCL Healthcare Biomagnetic and Nanomaterials Laboratories, 21 Albemarle Street, London, W1S 4BS, UK.*

[c.] *Department of Medical Physics and Biomedical Engineering, University College London, Gower Street, London, WC1E 6BT, UK.*

[d.] *Molecular Imaging and Innovative Therapies (IMOTION), Univ. Bordeaux, EA7435, Bordeaux, 33000, France.*

[e.] *Laboratoire de Chimie des Polymeres Organiques (LCPO), Univ. Bordeaux, CNRS, Bordeaux INP, UMR 5629, 33600 Pessac, France.*

Supplementary:

1. Intracellular MNPs quantification

To be able to compare both treatment methods, the concentration of nanoparticles used during the hyperthermia treatment must be the same. In order to determine what is the amount of nanoparticle being internalised by the cells after 24 h, the number of cells at the time of the hyperthermia treatment is essential. Under optimal conditions, a cell population in a culture will increase exponentially. Exponential growth of a cell population N at the growth rate r, as time t goes on in discrete intervals can be expressed by equation:

$$(t) = N_0\,(1 + r)$$

Where N_0 is the number of cells at time 0. The growth rate could be easily determined from counting cells from a passage to the next one. Therefore, the cell number at the time of the hyperthermia treatment could be calculated and was found to be equal to 600,000 cells. Previously cellular uptake of the MNCs using a SQUID magnetometer was quantified in Table 1. Under the same conditions, it was shown that an average of 125 pg (Fe_3O_4)/cell was internalised. Thus, it can be concluded that a total of 75 µg of MNCs is internalised in the cells.

2. The real-time heating curve of intracellular and extracellular thermo-chemotherapy.

The heating curves have been produced by recording the temperature during the AMF application and after the NPs internalisation. The oscillations of the temperature observed in every curve is due to the cooling water running through the inductor coil used to avoid parasitic heating and to maintain the cell sample at physiological temperature 37 °C or other value chosen for the test.

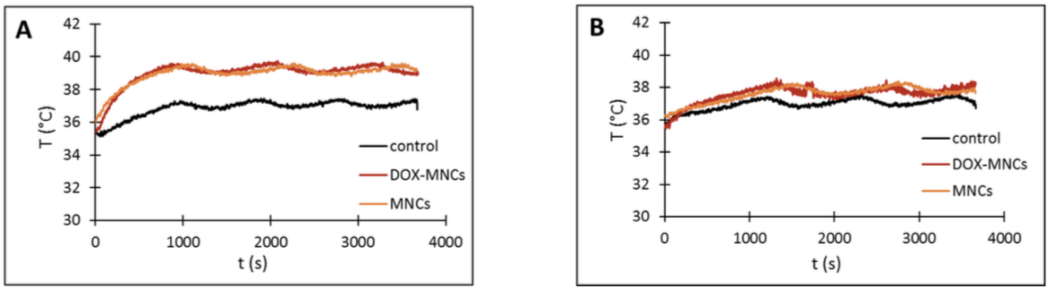


Figure. S1 A) U-87 cells and B) MCF-7 cells suspensions dispersed in DMEM supplemented with 10% FBS after internalisation of MNCs or DOX-MNCs and subjected to an AMF (f = 950 kHz and H = 10.5 kA/m). Control cells were not treated with nanoparticles.

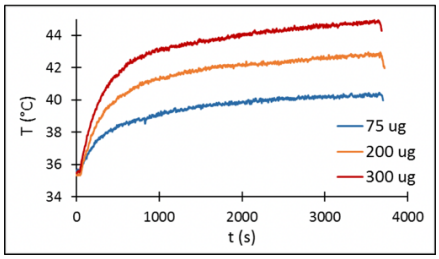


Figure. S2 Local environment temperature of cells suspensions dispersed in DMEM supplemented with 10% FBS containing 75 µg, 200 µg or 300 µg of MNCs and subjected to an AMF (f = 950 kHz and H = 10.5 kA/m).